The wobbling motion of single and two inline bubbles rising in quiescent liquid 🔵EP

🆔 **Yuanwei Cao (曹元伟) and Rafael Macián-Juan**

COLLECTIONS

EP   This paper was selected as an Editor's Pick

View Online   **Export Citation**   **CrossMark**

ARTICLES YOU MAY BE INTERESTED IN

The wobbling motion of single and two inline bubbles rising in quiescent liquid ᴇᴘ

Yuanwei Cao (曹元伟),[a) iD] and Rafael Macián-Juan

AFFILIATIONS

Institute of Nuclear Engineering, Department of Mechanical Engineering, Technische Universität München (TUM),
85748 Garching bei München, Germany

[a)]Author to whom correspondence should be addressed: yuanwei.cao@tum.de

ABSTRACT

The wobbling motions of single and two inline bubbles rising in quiescent liquid are investigated via three-dimensional simulations using the volume of fluid method. First, we simulate an 8 mm air bubble rising in quiescent water, yielding the wobbling motion. The bubble wobbling has two roles: (1) the excessive curvature speeds up the separation of the boundary layer and (2) the velocity peaks (high Reynolds number) result in the formation of asymmetrical vortices. The oscillation frequencies (6 Hz, $St = 0.22$) of the bubble movement, the vorticity accumulated on the bubble surface, the lift force and viscous force are the same while the oscillation frequency of the aspect ratio is twice that of the bubble movement. The volume-averaged liquid velocity presents a linear increase with the bubble rise while the kinetic energy displays a quadratic increase. Finally, two bubbles rising inline are investigated with different initial distances. The central breakup of the trailing bubble is observed at a short distance of 2d (d is the bubble diameter). For a longer distance of 6d, the wake of the leading bubble results in the lateral motion of the trailing bubble, depending on the position of the trailing bubble in the wake and the intensity of the vortices it encounters.

I. INTRODUCTION

Bubbles rising in liquids are encountered in many engineering applications, including the chemical engineering, nuclear industry, enhanced oil recovery, and so on.[1,2] The rising bubbles in liquid can yield different shapes, paths, and wakes[3] due to the coupled effect of gravity, surface tension, and liquid inertia.[4] Among others, the wobbling motion with path instability has motivated numerous investigations[5] due to its complexity. However, there are still open questions about the path instability, the velocity oscillation, and the interaction of the bubble with the wakes. Therefore, the main objective of this research is to deepen the understanding of these phenomena.

The path instability of single bubble rising in liquid is studied in numerous research studies.[6,7] Winnikow and Chao[8] obtained two wake regimes for a bubble rising. The bubble in the first regime forms a stationary wake while oscillations and periodic vorticity discharges were observed in the second regime. They suggested that the transition between the non-oscillating and oscillating regimes happens at the critical Weber number (We) of 4. Ryskin and Leal[9] thought that the vortex shedding leads to the path instability. Duineveld[10] confirmed for the first time that the bubble presented an oscillatory path in water when the bubble radius is bigger than 0.91 mm by using

hyper-purified water. Tomiyama et al.[11] conducted experiments using air and water to measure bubble trajectories, shapes, and velocities. They found that the primal cause of widely scattered terminal velocity in this regime is the initial shape. Small initial shape deformation resulted in a low velocity and a high aspect ratio. However, in the work of de Vries,[12] no vortex shedding in a region of path instability was found. Veldhuis et al.[13] studied the air bubbles rising in purified water. They found that the oscillations are indicated as (2,0) axisymmetric with wavelength equal to the distance from pole to pole and (2,2) non-axisymmetric and with wavelength equal to one-half of the length of the equator. By ruling out the contamination effect, Wegener et al.[14–16] conducted a series of experiments about the oscillating bubbles. In addition to the monitoring of the change between oscillating regimes at a critical We, an additional transition for the water/toluene system was also observed. For a certain diameter range with $We < We_{cr}$, they found that bubbles suffer a sharp reduction in rise velocity right after initial acceleration and then oscillate. In the work of Tripathi et al.,[3] they identified five distinct regimes with sharply defined boundaries based on their 3D simulations of single bubble rising in quiescent liquid. However, whether vortex shedding leads to path instability or vice versa is still

not clear. Therefore, some aspects of single bubble rising with path instability are still not resolved.

The dynamics of two inline bubbles have also been a subject of research due to their complex interaction of the trailing bubble (TB) with the wake generated by the leading bubble (LB). In the numerical work of Yuan and Prosperetti,[17] they simulated two undeformable spherical bubbles moving along the centerline using axisymmetric configuration. An equilibrium distance was found at which the wake effect and the repulsion pressure balance each other. Later on, Watanabe and Sanada[18] showed that the deformable inline bubbles rise with a stable equilibrium distance when the initial distance is at least 2.5d (d is the bubble diameter) through their axisymmetric simulations. However, Katz and Meneveau[19] demonstrated experimentally that the bubble pairs can attract and collide. When the initial distance of the two inline bubbles is 1.5d or more, the terminal speed of TB increases and the distance between them decreases while LB is almost unaffected by TB. The mismatch between the reported numerical and experimental results is due to the presence of the bubble deformation, impurities, and three-dimensional features.[20,21]

Most of the works mentioned above mainly studied the bubble rising in a straight path.[22] Few research studies focus on the study of two inline bubbles rising in liquid with path instability. Hallez and Legendre[23] studied the flow around a pair of bubbles with various relative angles numerically. They showed that a strong shear-induced lift force in the wake of LB acts on TB. Gumulya et al.[24] reported TB deviation owing to interaction-induced wake instability. Kusuno et al.[25] conducted experiments on the motion of a pair of bubbles initially positioned in line, and two effects were observed. The first one is potential effects at a short distance between bubbles, and the second is the wake of the leading bubble. Fillela[26] presented an experimental study of the hydrodynamic interaction between two bubbles rising at high Reynolds numbers. Two main effects were highlighted: (1) the role of the ascending flow generated by the leading bubble and (ii) the role of the vortices released by LB inducing strong localized horizontal deviations on TB. However, the numerical research on two inline bubbles with path instability at high Re is still missing. Therefore, another objective of the present research is about the numerical investigation of two inline bubbles with path instability.

For this purpose, we carry out high-resolution three-dimensional time-dependent simulations on single and two inline bubbles rising in quiescent liquid. The paper is organized as follows. The main features of the numerical model and dimensionless numbers are presented in Sec. II. The main results of the wobbling motion of isolated and two inline bubbles in quiescent liquid are covered in Secs. IV and V, where the mechanism of the wobbling motion of isolated bubbles is clarified. Two inline bubbles rising with different initial distance are investigated quantitatively. Finally, Sec. VI is devoted to the general summary and conclusion.

II. MATHEMATICAL FORMULATION
A. Governing equations

All the simulations presented in this work are conducted with interIsoFoam solver implemented in OpenFOAM v1806, which adopts the geometric VoF method. The governing equations to solve two isothermal, incompressible, immiscible fluids with variable density and viscosity including continuity, momentum, and interface advection equations are[4]

$$\nabla \cdot \mathbf{U} = 0, \tag{1}$$

$$\frac{\partial \rho \mathbf{U}}{\partial t} + \nabla \cdot \rho \mathbf{U}\mathbf{U} - \nabla \cdot \mu \nabla(\mathbf{U}) = \mathbf{F_\sigma} - \mathbf{g} \cdot \mathbf{x}\nabla\rho - \nabla p_d, \tag{2}$$

$$\frac{\partial \alpha}{\partial t} + \nabla \cdot (\alpha \mathbf{U}) = 0, \tag{3}$$

where $\mathbf{U}$ is the velocity vector, $\mathbf{F_\sigma}$ is the surface tension force, $\mathbf{g}$ is the gravitational acceleration, t is the time, and $p_d = p - \rho \mathbf{g} \cdot \mathbf{x}$ is the dynamic pressure used to avoid any sudden changes in the pressure at the boundaries for hydrostatic problem.

At each computational cell, the volume fraction, α, is defined as the ratio of one fluid volume to the volume of cell:

$$\alpha(\mathbf{x}, t) = \frac{V_{Liquid}}{V} = \begin{cases} 1, & \mathbf{x} \in \text{Liquid}, \\ 0 < \alpha < 1, & \mathbf{x} \in \text{interface}, \\ 0, & \mathbf{x} \in \text{gas}. \end{cases} \tag{4}$$

The density and viscosity in each cell are calculated through α,

$$y = \alpha y_L + (1 - \alpha)y_G, \quad y \in [\rho, \mu], \tag{5}$$

where L and G are the liquid and gas phase, respectively.

The mentioned governing equations are discretized by using the finite volume method (FVM) in the OpenFOAM package.[27] The solution of the discretized momentum equation is performed by constructing a predicted velocity field,[28] and it was corrected using the Pressure Implicity with Splitting Operator (PISO)[29] algorithm to time advance the pressure and velocity fields in Eq. (2). The interface capturing methodology used here to solve Eq. (3) is called isoAdvector, a geometric VoF method developed by Roenby et al.[30] This method uses the concept of iso-surface to calculate the face fluxes for the cells containing the interface. The detailed description of the isoAdvector algorithm and the evaluation can be found in Ref. 30.

B. Dimensionless numbers

The dimensionless numbers to determine the bubble dynamics appeared in the paper, the Galilei number (Ga), Eötvös number (Eo), Reynolds number, and Strouhal number (St), are defined as

$$Ga = \frac{\rho_0 \sqrt{g} R^{3/2}}{\mu_0}, \tag{6}$$

$$Eo = \frac{\rho_0 g R^2}{\sigma}, \tag{7}$$

$$Re = \frac{\rho_0 U_b d}{\mu_0}, \tag{8}$$

$$St = \frac{f d}{U_T}, \tag{9}$$

where R is the radius of the bubble, σ is the surface tension coefficient, and ρ_0, μ_0 and ρ_i, μ_i are density and viscosity of the continuous and dispersed phases, respectively. U_b is the bubble rising velocity. f is the oscillation frequency of the path, d is the bubble diameter, and U_T is the bubble terminal velocity. The Ga number represents the ratio of gravity force to viscous force, and the Eo number represents the ratio of gravity force to surface tension force. The Re number is the ratio of inertial force to viscous force. In some studies,[3] they use the Ga instead of Re since the bubble rising velocity is not known a priori. The St number is used to describe the oscillating flow mechanisms.

TABLE I. The physical parameters of skirted bubble in the work of Sharaf et al.[31]

	Density (kg/m³)	Viscosity (mPa s)	Surface tension (kg/s²)	Eo	Ga
Liquid	1254	967.8	0.0624	73.28	10.86
Gas	1	0.0151			

TABLE II. The setting of boundary conditions.

Boundary	Volume fraction	Pressure	Velocity
Bottom wall	Zero gradient	Fixed flux pressure	Fixed value (0 0 0)
Top wall	Inlet outlet	Total pressure	Pressure inlet outlet velocity
Side walls	Zero gradient	Zero gradient	Slip

III. VALIDATION AND MESH INDEPENDENCE STUDY

Before proceeding to the investigation of the wobbling motion of single and two inline bubbles, the solver must be validated, and the mesh resolution should be confirmed with published experimental data.

A. Skirted bubble

The first validation case is chosen from the experimental results of Sharaf et al.,[31] which has also been adopted in our previous work.[4,32] The numerical domain is a cuboid with the dimension of $6d \times 6d \times 15d$ (d is the bubble diameter), in which a structured hexahedral mesh is used. The physical parameters are displayed in Table I. Atmosphere and wall boundary conditions are set for top and bottom boundaries, while slip boundary conditions are used on the cuboid wall.

The simulation results with different mesh resolutions are compared to the experimental data as shown in Fig. 1. Z_{tip} is the bubble-tip position normalized with the equivalent radius of the bubble, and the dimensionless time is normalized with $\sqrt{R/g}$. We can see that the result of mesh size d/20 is already converged. The comparison of

bubble shape evolution between present numerical results and experimental results is shown in Fig. 1, which displays a good agreement.

B. Oscillatory bubble

To simulate the path instability, the interface and the wake structure must be fully resolved, which is dependent on the mesh resolution. Thus, a mesh independence study should be conducted. In this section, we simulate an air bubble with a diameter of 8 mm. The numerical domain for the simulation of the rising bubble with path instability is a cuboid fluid domain with a size of $6d \times 6d \times 50d$ m³ (d is the bubble diameter) filled with water. Atmosphere and wall boundary conditions are applied on the top and bottom boundaries while slip boundary conditions for all the vertical walls (Table II). The bubble is initially located at $1.5d$ above the bottom wall. The physical properties of the two phases are listed in Table III. All the computations are performed on a structured hexahedral mesh.

The mesh sizes are $\Delta x = d/[20, 30, 40]$. The time step is set as $\Delta x/10$ and the Courant number is 0.5. The results of the center of
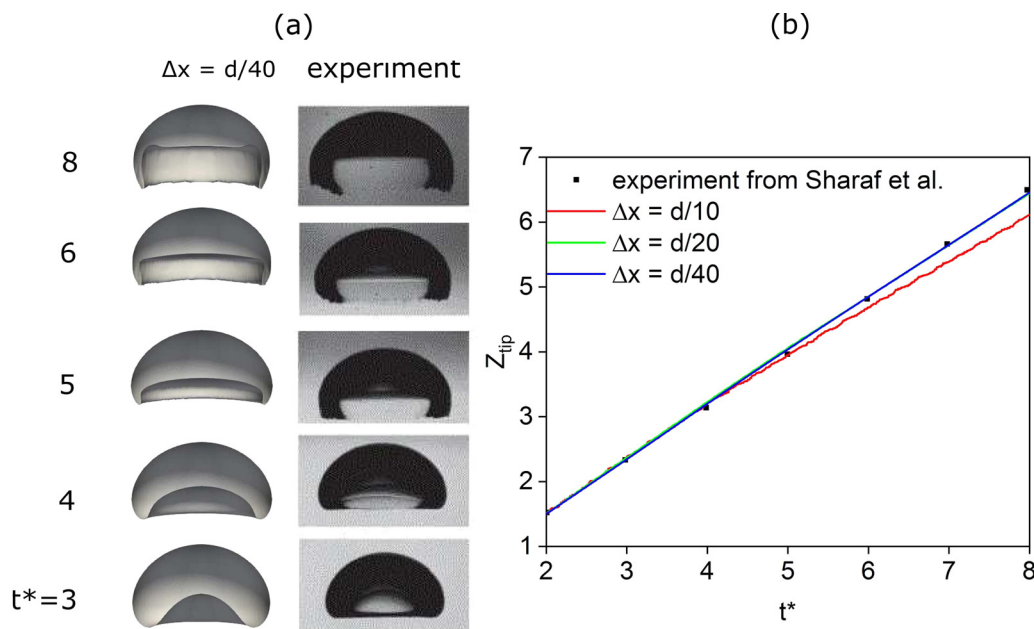

FIG. 1. (a) Comparison of the bubble shape evolution between experimental[31] and present numerical results. (b) Comparison of the temporal variation of Z_{tip} obtained from different mesh size and the experimental results. The results are reproduced with permission from Cao and Macián-Juan, Phys. Fluids **32**(3), 033302 (2020). Copyright 2020 AIP Publishing.

TABLE III. The physical properties of the two phases.

phase	ρ (kg/m^3)	μ (mPa s)	σ (kg/s^2)	Ga	Eo
Water	998	1	0.073	790.78	2.15
Air	1.2	0.0151			

TABLE IV. Comparison of the terminal velocity and aspect ratio with the experimental data.[34]

	V_T (m/s)	E
Simulation	0.209	0.55
Experiment	0.212	0.6

mass for different mesh sizes are shown in Fig. 2. The center of mass is made dimensionless with the bubble diameter ($Z^* = Z/d$) and the dimensionless time is normalized with $t' = t/\sqrt{d/g}$. From Fig. 2, we can see that the results of mesh size $d/30$ are already converged. In consideration of the work of Tripathi et al.[3] and Zhang and Ni,[33] the mesh size of $d/32$ is chosen for the following simulations in this work.

Then the terminal velocity (V_t) and aspect ratio (E) from our simulation results are compared to the experimental data of Liu et al.,[34] which is shown in Table IV. The terminal velocity is obtained when the bubble rising velocity reaches a constant value. The bubble rising velocity is defined as

$$V = \frac{\int_{\alpha<0.5} \mathbf{U} dV}{\int_{\alpha<0.5} dV},\tag{10}$$

where $\mathbf{U}$ is the instant vertical velocity in a particular cell. The aspect ratio is calculated as $E = d_Z/\sqrt{d_X d_Y}$, where d_X and d_Y are the major axes of the bubble, and d_Z is the minor axis. The relative errors of V_t and E are 1.4% and 8.3%, which supports the validity of the current numerical approach and mesh resolution.

IV. SINGLE OSCILLATORY BUBBLE

In this section, the mechanism of the path instability is elucidated with the validated case in Sec. III B. The trajectory normalized with bubble diameter of the bubble is displayed in Fig. 3, which is rather chaotic and agrees with the findings in Gumulya et al.[35] The hydrodynamics of a single bubble with path instability are highly relevant to the bubble shape deformation, wake development, and the transverse forces exerted on the bubble,[36] which are analyzed in the following parts within this section.
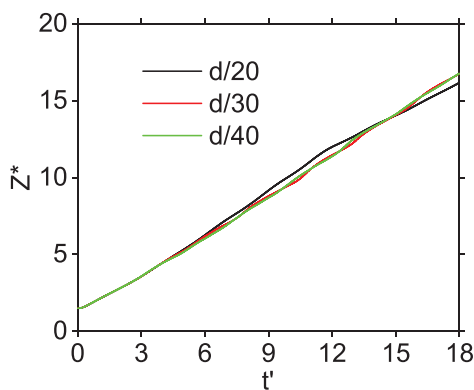
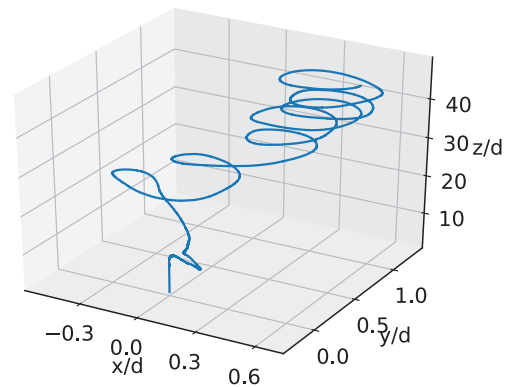**FIG. 2.** The mesh independence study for the path instability.

FIG. 3. The trajectory of an air bubble rising in quiescent water (non-dimensionalized with bubble diameter).

The temporal variations of the rising velocity and aspect ratio are shown in Fig. 4. The velocity is made dimensionless with $V^* = V/\sqrt{gd}$[37] due to the high Re (≈ 2000, see below). Before the analysis of the path instability, the velocity oscillation appeared in Fig. 4(a) is first examined as we think it promotes the formation of the asymmetric vortex in the rear of the bubble, which contributes to the occurrence of the path instability. Once the air bubble is released in the water, it rises due to the buoyancy and a boundary layer around the bubble is formed. The water motions are completely driven by the bubble rise. Due to the interaction of inertia and surface tension force, the bubble wobbling is observed as shown in Fig. 4(b). We think that the bubble wobbling has two roles: (1) the excessive curvature speed up the separation of the boundary layer and (2) the velocity peaks (high Re) result in the formation of asymmetrical vortices. The maximum velocity can reach 1.26 at $t' = 8$, corresponding to the Re ≈ 2000. Then the vortices are not formed symmetrically at some point and different lift forces develop on each side of the bubble, which results in the bubble motion transverse to the flow.

As a further analysis, we calculate the bubble movement, the vorticity accumulated on the bubble surface, the lift force and viscous force exerted on the bubble (all in X and Y directions), which is shown in Fig. 5. Then the hydrodynamics of the rising bubble with path instability are analyzed. The vorticity components in X and Y directions accumulated on the bubble surface are calculated as $\tau_{(X,Y)} = \int_s \omega_{(X,Y)} dS$, where S is the bubble interface and $\omega_{X,Y}$ is the vorticity component in X and Y directions. The lift force is calculated as $F_{(X,Y)} = \int_s p \cdot \mathbf{n}_{(X,Y)} + \tau_{(X,Y)} dS$, where p is the pressure, $\mathbf{n}_{X,Y}$ is the bubble surface normal direction, and $\tau_{X,Y}$ is the viscous force. We can observe that the oscillation frequencies (6 Hz, St = 0.22) of the bubble movement, the vorticity
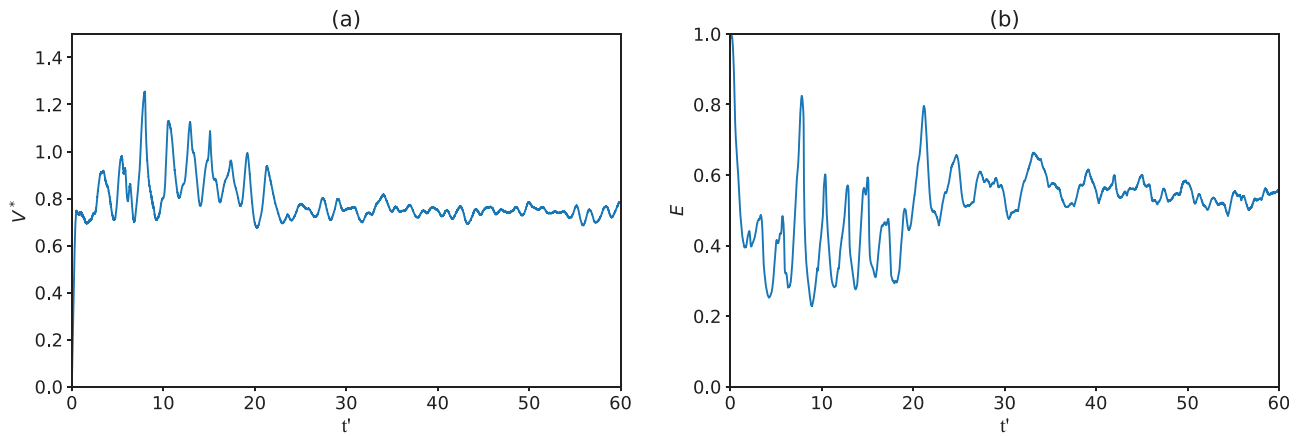
FIG. 4. The temporal variations of (a) the terminal velocity and (b) aspect ratio.

accumulated on the bubble surface, the lift force, and viscous force are the same. In the straight path, the oscillation amplitude of these variables is all 0, which means a symmetric flow field. After $t' = 8$ ($V^* = 1.26$), the forces exerted on the bubble seem to oscillate first, earlier than that of the bubble movement and the vorticity. Afterward, the accumulated vorticity on the bubble surface seems to oscillate followed by the horizontal bubble movement. Therefore, after the pressure loses symmetry, the vorticity and bubble movement begin to oscillate, which means the happening of the path instability. Compared to the contribution of the pressure, the influence of the viscous force (10^{-6}) on the path instability is negligible due to the large Re.

Figure 6 shows the bubble shape evolution and the vortex structures during the wobbling. We can observe that the bubble wobbling

mainly manifests in the vertical length variation of the bubble in Fig. 6(b). The longest vertical length ($t' = 8$ and $t' = 10.5$) corresponds to the velocity maxima. As discussed in our previous paper,[4] the liquid jet in the rear of the bubble with higher velocity than the bubble rising velocity, resulting from the pressure difference between the top and bottom of the bubble, can "push" the bubble and increase the bubble rising velocity. In the meantime, the liquid jet can also compress the bubble (cannot penetrate the bubble due to the surface tension force), decreasing the vertical length of the bubble, thus decreasing the liquid jet velocity. Here, we use the Q criterion[38] to identify the pure rotational motion in the liquid. The vortex structures revealed by Q criterion during the bubble wobbling are shown in Fig. 6(a). In Fig. 6(a), we carefully tune the Q values, and the hairpin structures
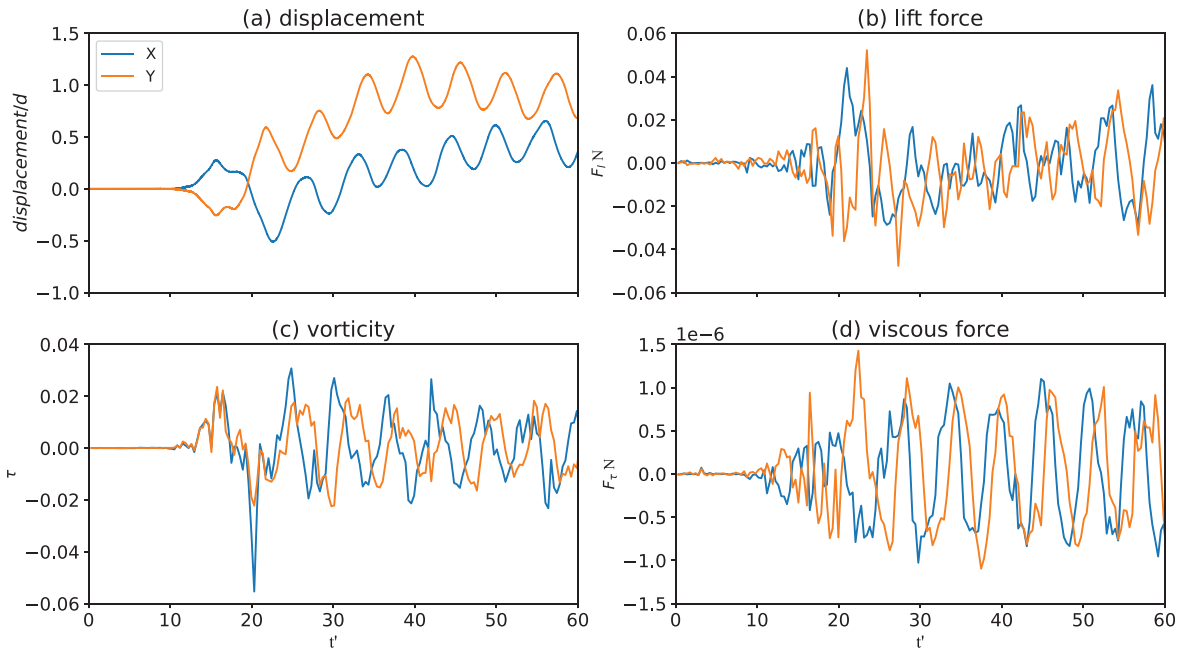

FIG. 5. The time history of (a) the displacement of the bubble, (b) lift force, (c) the vorticity accumulation on the bubble surface, and (d) viscous force in X and Y direction.
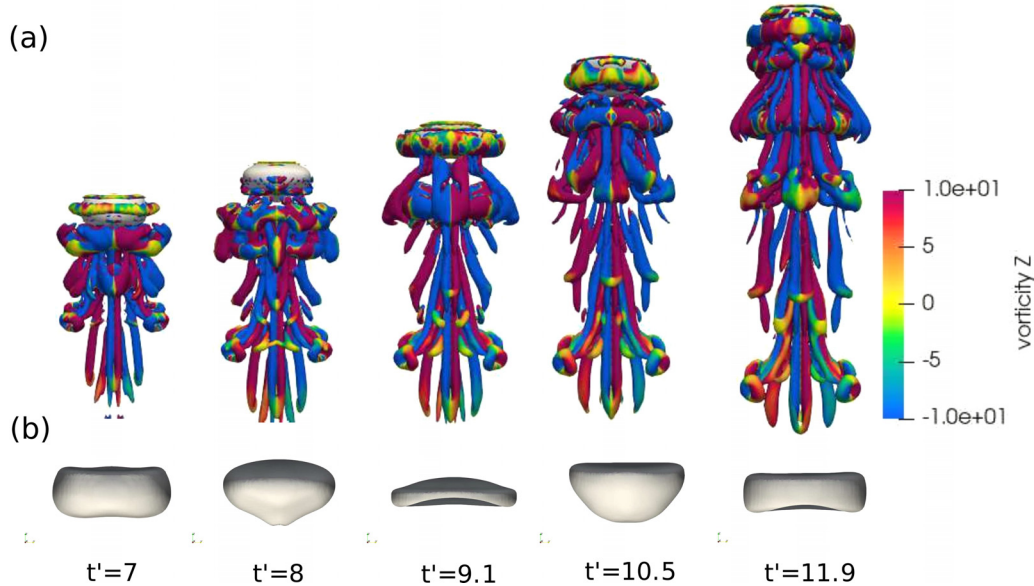
FIG. 6. (a) The vortex structures revealed by Q criterion (Q = 10) and (b) the bubble shape at different time instants. The iso-vortices are colored with ω_z.

are observed. In classic wall turbulence flows, hairpin vortices are widely studied as an important structural aspect. The hairpin structures control the turbulent motions by the parent-offspring mechanism by generating a series of hairpins one after another.[39] As the bubble rises, a toroidal vortex ring is formed on the bubble surface ahead of the maximum diameter plane and develops further to the rear side of the bubble. At the stagnation point in the rear side of the bubble, a low pressure zone is created and the hairpin structures appear in the flow.[21] The hairpin legs are still attached to the bubble while the legs point downward. Four hairpin legs can be observed in our simulation. With the bubble wobbling, more hairpin vortices are generated and interact with each other, which forms a flower-like structure. The flower-like structure bursts with the bubble wobbling and ejects small scale liquid motions.

Here, we also display the wake structures of the rising bubble in the spiral motion after $t' = 20$ (Fig. 7). At $t' = 20$, the legs of the old hairpin vortex are still attached to the rear bubble surface. At the same

time, new hairpin vortices are also formed. At $t' = 60$ in the fully developed spiral motion, the hairpin vortices are observed in the spiral path induced by the rising bubble. Many hairpin structures are tilted and interact with one another. The occurrence of the path instability is also related to the shape oscillations in addition to the bubble wake. We analyzed the bubble movement in Y direction and find that the oscillation frequency of the aspect ratio E (d_Z/d_Y) is twice that of the bubble movement in the Y direction. Actually, the shape oscillation of the bubble is considered to be of an effect of the path instability, caused by the uneven pressure distribution about the equatorial plane of the bubble during the spiral motion.

As the bubble rises, energy is transferred from the bubble to the liquid phase, generating a wide range of small and large scale of motion which may also create turbulent motion (bulk generated turbulence).[36] Thus, it is necessary to measure the momentum and kinetic energy received by the liquid phase. Here, the agitation created in the liquid is quantified with the volume-averaged velocity
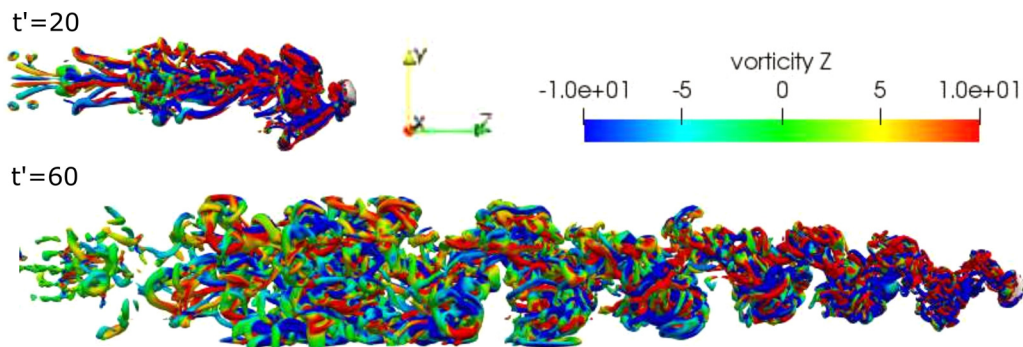

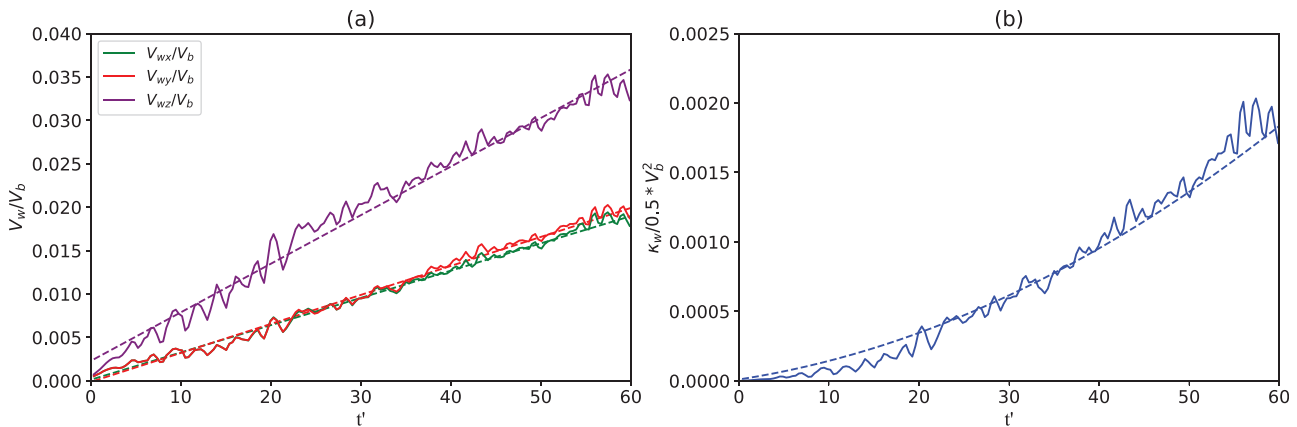**FIG. 7.** The vortex structures extracted using the Q criterion (Q = 10) at $t' = 20$ and $t' = 60$.

FIG. 8. The time history of (a) the volume-averaged liquid velocity and (b) the dimensionless liquid kinetic energy.

fluctuation,[21] $\langle \mathbf{u} \rangle = \int_V mag(\mathbf{u})dV$, where $\mathbf{u}$ is the velocity vector in the liquid phase and V is the total liquid volume. The dimensionless volume-averaged total kinetic energy per unit mass in the liquid is calculated as, $\kappa_w = (u_x^2 + u_y^2 + u_z^2)/V_b^2$. The components of the volume-averaged liquid velocity and the dimensionless volume-averaged kinetic energy are shown in Fig. 8. We can observe that the velocity fluctuations in vertical direction are more intense than that in the lateral direction, all of which present a linear increase until $t' = 55$. After that, the velocity fluctuates around a stable value. From Fig. 8(b), the dimensionless kinetic energy presents a quadratic increase until $t' = 55$ and after that it fluctuates around a stable value.

V. TWO INLINE BUBBLES WITH PATH INSTABILITY

In this section, we simulate and analyze the wobbling motion of two inline bubbles. When the bubble-wake interaction happens in different positions of the bubble rising path, the rising bubble dynamics will be different. Therefore, we simulate three cases: (1) $h = 2d$ (h is the distance of the leading and trailing bubble center); (2) $h = 4d$; and (3) $h = 6d$. However, the bubble coalescence is not the objective of the present research and we only investigate the bubble-wake interaction before the coalescence.

A. $h = 2d$

For case 1 ($h = 2d$), the two bubbles interact mainly in the straight rising path. The rising velocity of the two bubbles and the shape evolution are shown in Fig. 9. Before $t' = 5$, TB and LB rise with the same velocity since TB has not interacted with the wake flow of LB. After $t' = 5$, TB enters the wake region created by LB. We can observe the velocity increase in TB due to the added mass effect from $t' = 5$ to the coalescence of the two bubbles as shown in Fig. 9(a). The approach of the two bubbles is displayed in Fig. 9(b). TB is elongated at $t' = 6.6$ as it approached LB. Based on the discussion in Refs. 4 and 40, this phenomenon is caused by the shielding effect of the wake flow behind LB. Because of the elongation of TB, the velocity of the liquid jet caused by the pressure difference between the top and bottom of TB[32] becomes larger, resulting in the central breakup of TB [at $t' = 7.4$ in Fig. 9(b)].
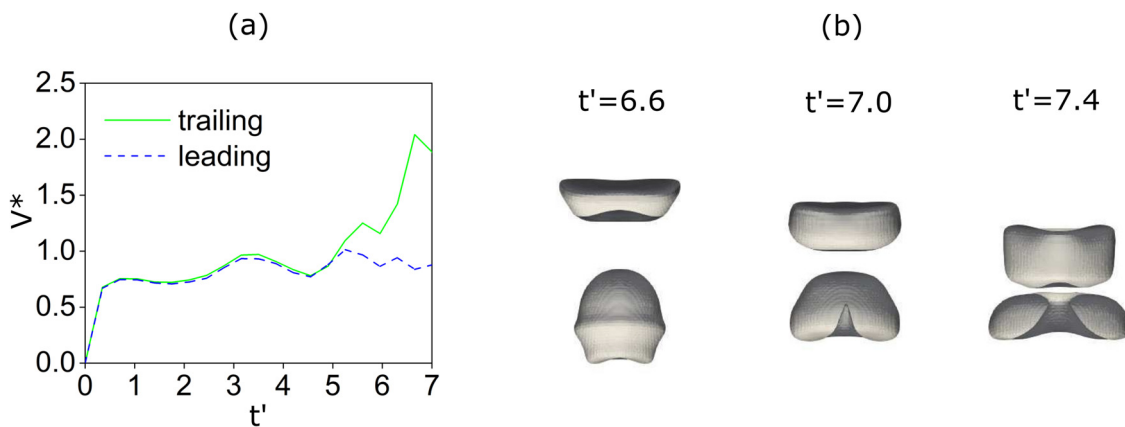

FIG. 9. (a) The time history of the rising velocity of the two bubbles with $h = 2d$ and (b) the bubble shape evolution.
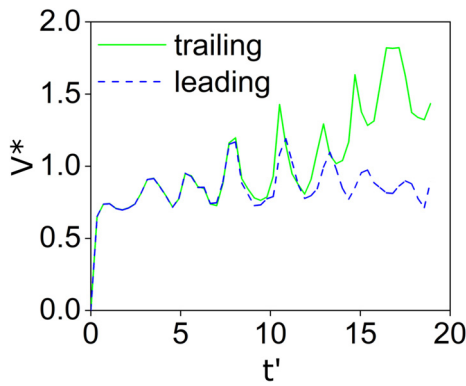
FIG. 10. The time history of the rising velocity of the two bubbles with $h = 4d$.

FIG. 12. The evolution of the vortex structures revealed by Q criterion ($Q = 10$) with $h = 4d$.

B. $h = 4d$

For case 2 ($h = 4d$), the two bubbles interact in the straight rising path and the transition phase. We plot the rising velocity of the two bubbles in Fig. 10. From $t' = 0$ to $t' = 10$ in the straight rising path, the rising velocities of the two bubbles are almost the same, meaning no interplay of the two bubbles. From $t' = 10$ to $t' = 14$, the velocities of the two bubbles are still oscillating due to the bubble wobbling. However, the velocity of TB is slightly higher than that of LB. Therefore, the bubble wobbling caused by the interaction of inertia force and the surface tension force dominates in this period compared to the interaction of the two bubbles. From $t' = 14$ to $t' = 20$ (bubble coalescence), the rising velocity of TB is comparatively higher than that of LB. In this period, the interaction of TB with the wake flow of LB plays a more important role in the bubble motion. However, the velocity oscillation can still be observed, and oscillation amplitude ($\Delta V = 0.5$) of TB is larger than that ($\Delta V = 0.2$) of LB.

We plot the evolution of the streamlines of the two bubbles in Fig. 11. At $t' = 7$, the two bubbles are far away from each other,
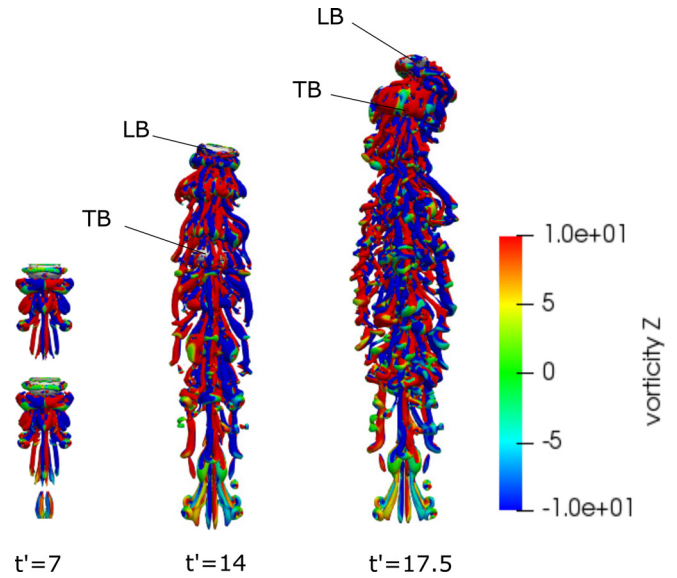
and they do not interplay. From $t' = 10$, TB enters the flow region which is affected by the rising of LB. Due to the added mass effect, TB starts to accelerate. As TB approaches LB, the vortexes generated by LB merge into the ones generated by TB ($t' = 14$ in Fig. 11). Since the distance between the TB and LB is short when they enter the path instability, the effect of the wake generated by LB on TB is not obvious, and no horizontal deviation is observed for TB $t' = 17.5$.

The wake structures revealed by Q criterion during the rising of the two inline bubbles ($h = 4d$) are displayed in Fig. 12. At $t' = 7$ when TB and LB do not interplay, the wake structures of the two bubbles are the same to that of a single bubble and the flower-like
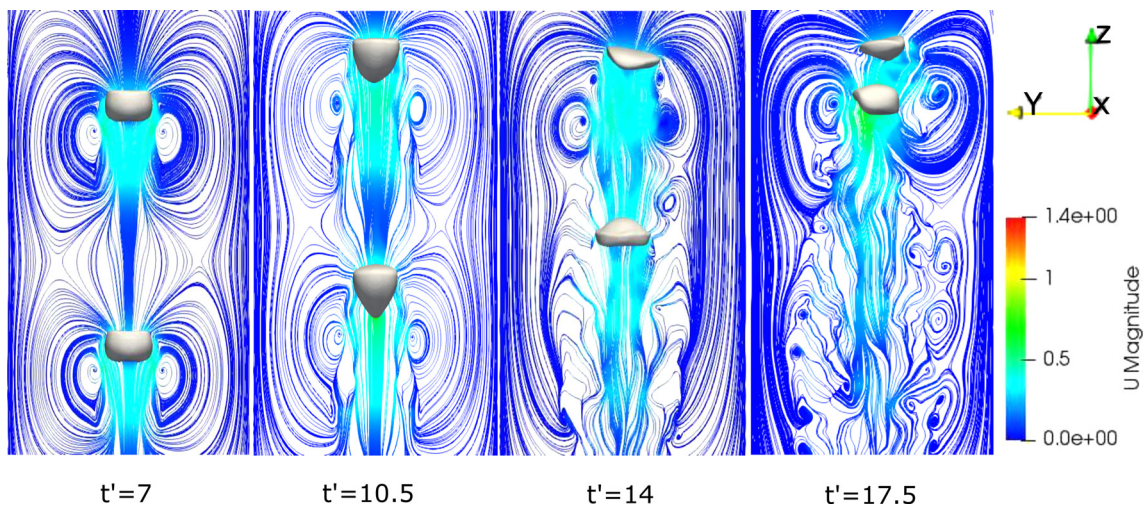

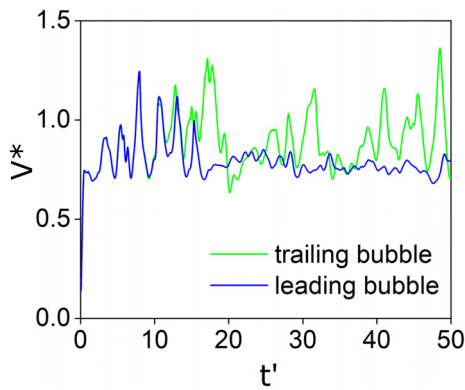FIG. 11. The evolution of the streamline of the two bubbles.

FIG. 13. The time history of the rising velocity of the two bubbles with $h = 6d$.

structures can be observed. At $t' = 14$, TB interacts with the wake generated by LB in the straight path, which affects the rising velocity of TB as seen in Fig. 10. At $t' = 17.5$ before the coalescence, LB rises with path instability and the lateral motion of TB seems to be

slightly delayed due to its interaction with the wake of LB. In addition, more small-scaled hairpin structures can be observed at this time due to the rising motion of TB.

C. $h = 6d$

For $h = 6d$, the interaction of TB with the wake generated by LB becomes more complex. Depending on the position of TB in the wake of LB and the intensity of the vortices TB encounters, the path of TB can be more or less modified. In this section, we analyze the behavior of TB in the wake of LB.

We plot the time history of the rising velocity of the two bubbles in Fig. 13. Before $t' = 12$, the two bubbles rise with the same velocity. After that, the rising velocity of the two bubbles yields different tendency. The time history of LB is the same to that of a single rising bubble. However, the rising velocity of TB is much affected by the wake of LB, resulting in distinct oscillations with a larger amplitude. However, the average velocity of TB is still larger than that of LB because of the added mass effect from LB, which leads to the coalescence of the two bubbles in the end.
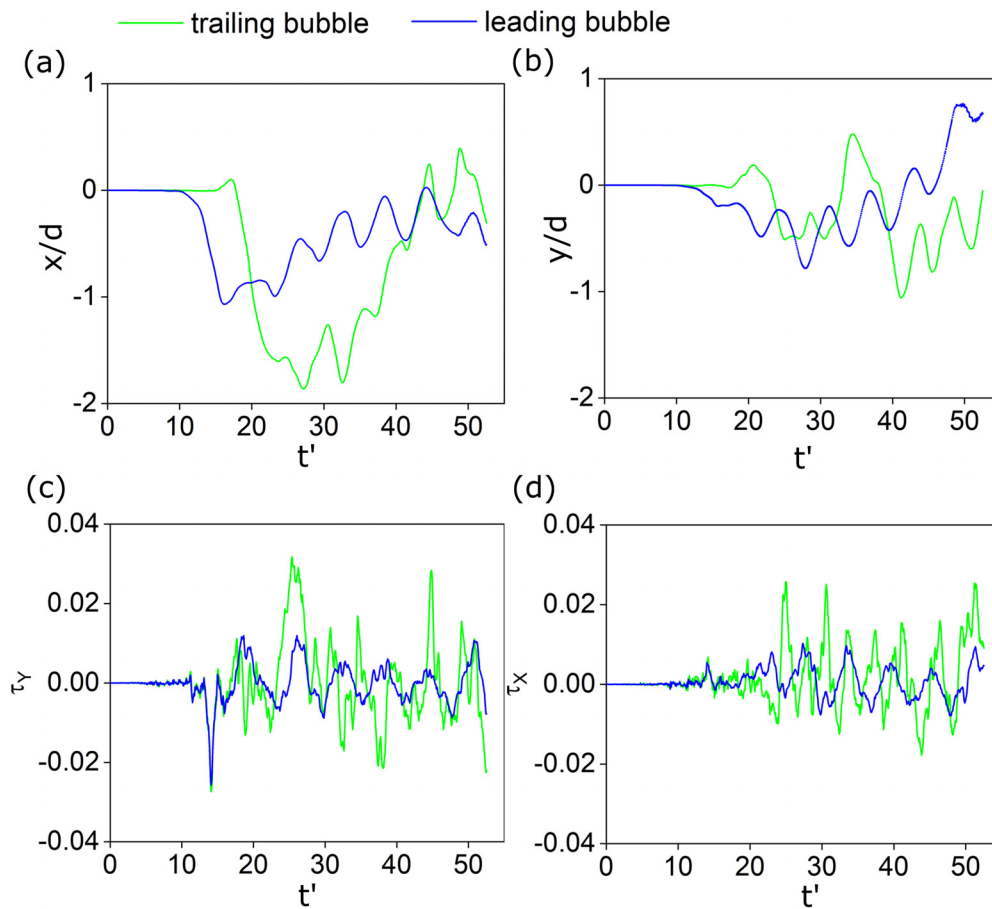

FIG. 14. The time history of (a) the bubble displacement in X direction, (b) the bubble displacement in Y direction, (c) the Y component of the accumulated vorticity, and (d) the X component of the accumulated vorticity of the two bubbles with $h = 6d$.
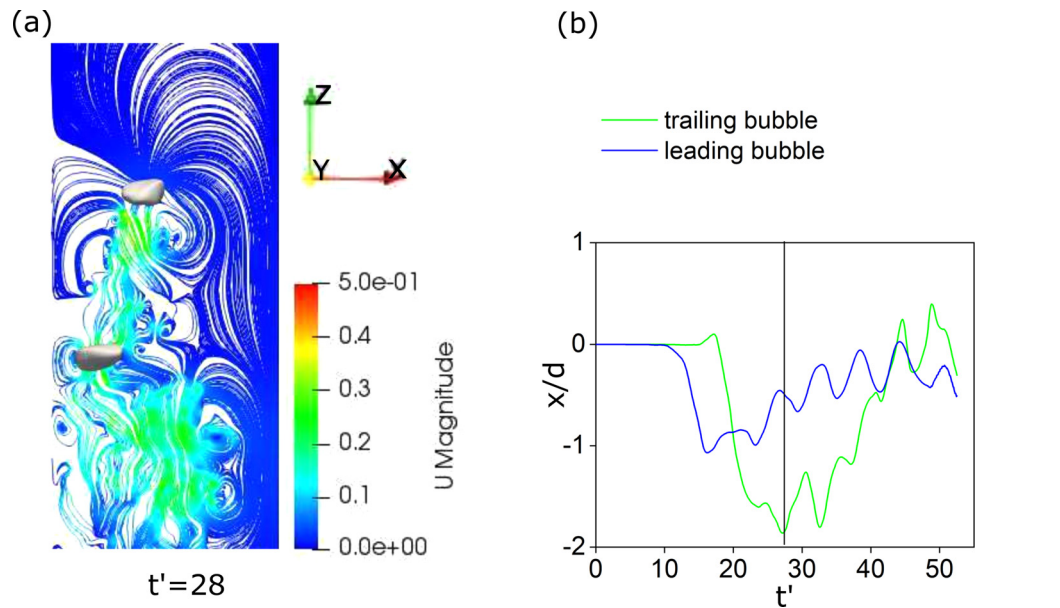
FIG. 15. Drift away of the trailing bubble. (a) Streamlines of the velocity field at the time of ejection $t' = 28$. (b) The time history of the bubble displacement in X direction.

The time history of the bubble displacement and the accumulated vorticity on the bubble surface are displayed in Fig. 14. Compared to LB, no periodicity of the displacement of TB is observed, and the oscillation amplitude is larger. Due to the interaction of TB with the wake shedding from LB, τ_X and τ_Y of TB are disordered due to the position of TB in the wake of LB, and the intensity of the vortices TB encounters.

The wake generated by LB can cause the lateral motion of TB, which results in the TB moving either toward the wake center or away from it[26,41,42] depending on the intensity and direction of the wake. These effects are shown in Figs. 15 and 16. In Fig. 15, TB is drifted from the center in the wake to the leftmost position at $t' = 28$ s. We can observe the horizontal drift of TB from Fig. 15(a). The inertial force driving TB toward the vortex core is sufficient compared to the buoyancy, which means that the horizontal velocity induced by the vortex is comparable to the terminal velocity of the bubble to yield the modification of the path of TB. Here, we measure the horizontal velocity V_x and terminal velocity V_Z at $t' = 20$, which are $V_X = -0.53$
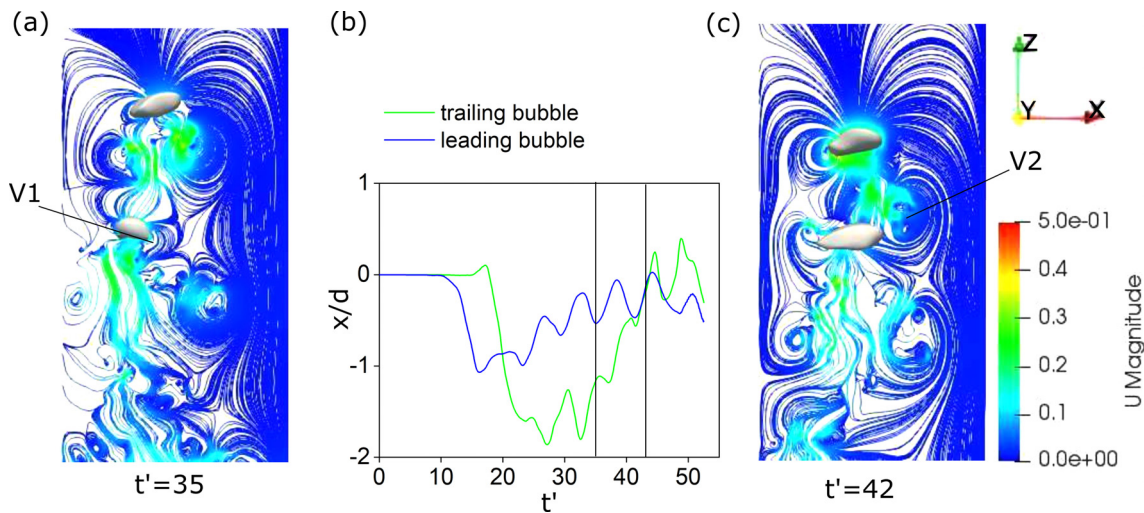

FIG. 16. Centering of the trailing bubble. (a) Streamlines of the velocity field at the time of centering $t' = 35$. (b) The time history of the bubble displacement in X direction. (c) Streamlines of the velocity field at the time of centering $t' = 42$.
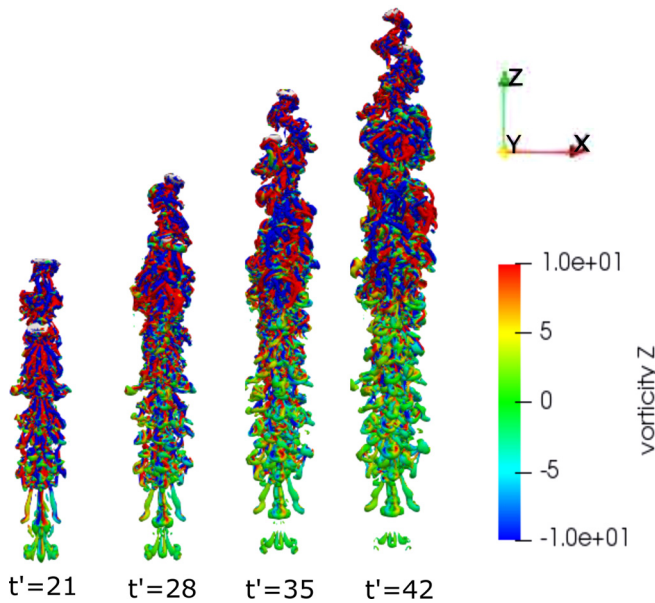
FIG. 17. The evolution of the vortex structures revealed by Q criterion (Q = 10) for two inline bubble rising with h) 6d.

and $V_Z = 0.67$. However, for a single bubble rising, the horizontal velocity V_X is only 0.077 at this time ($t' = 20$).

On the other hand, TB can also drift to the center of the wake, which is shown in Fig. 16. We can observe that TB enters the center of the wake progressively at $t' = 35$ and $t' = 42$. The horizontal velocity V_X and terminal velocity V_Z of TB are 0.16 and 0.80 at $t' = 35$, respectively. The horizontal velocity V_X of a single rising bubble is only 0.09. The inertial force induced by the vortex driving TB toward the center of the wake is not big enough compared to the buoyancy since the intensity of the vortex (V1 in Fig. 16) TB encounters is not strong. After that TB encounters the stronger clockwise rotational motion of the vortex [V2 in Fig. 16(c)] heading to the higher velocities in the ascending flux. At $t' = 42$, the horizontal velocity V_X of TB increases

to 0.32. Therefore, the centering of TB is a progressive process, it slowly drifts toward the center of the wake.[26]

The wake structures of the two inline bubble with h = 6d are shown in Fig. 17. We can see that the lateral motion of TB is greatly affected by the wake of LB. Depend on the direction and the strength of the vortex TB encounters, the trajectory of TB can either be toward the wake center of away from it. Due to the appearance of TB, more hairpin vortices are generated in the wake. We also calculate the momentum and kinetic energy received by the liquid phase from the two inline bubbles. The volume-averaged velocity fluctuation and total kinetic energy are shown in Fig. 18. Compared to the case of a single bubble, the liquid volume-averaged velocity created by two inline bubbles is doubled before TB enters the wake region of LB ($t' = 10$) and is less than the doubled value after TB enters the wake region of LB. The total liquid kinetic energy transferred from two inline bubbles is four times of that from single bubble before $t' = 10$ and less than the four times after that due to the wake effect of the LB.

VI. CONCLUSION

In this paper, the wobbling motions of a single and two inline bubbles rising in quiescent liquid are numerically studied via 3D simulations using the VoF method. The mechanism of the path instability of the wobbling bubble motion is analyzed. We also investigate the two bubbles rising in line with different initial distances.

The path instability is observed in the trajectory of an 8 mm air bubble rising in quiescent water, and the results are compared to the experimental data. The bubble wobbling has two roles: (1) the excessive curvature speeds up the separation of the boundary layer and (2) the velocity peaks (Re) result in the formation of asymmetrical vortices. The oscillation frequencies (6 Hz, St = 0.22) of the bubble movement, the vorticity accumulated on the bubble surface, the lift force and viscous force are the same while the oscillation frequency of the aspect ratio E is twice that of the bubble movement. The forces exerted on the bubble seem to oscillate first, earlier than that of the bubble movement and the vorticity. The hairpin structures are tilted and interact with one another during the spiral motion. The velocity fluctuations in the liquid phase in vertical direction are more intense than that in the lateral direction, all of
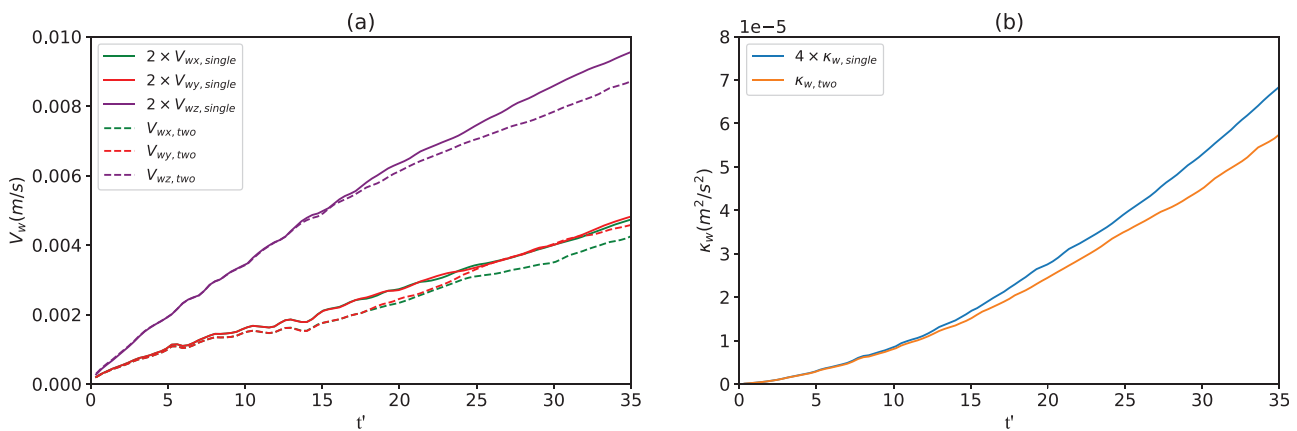

FIG. 18. The comparison of (a) the volume-averaged liquid velocity and (b) the dimensionless liquid kinetic energy between single and two inline bubbles.

which present a linear increase while the dimensionless kinetic energy presents a quadratic increase.

For two inline bubbles, three cases are considered with the initial distance $h = [2d, 4d, 6d]$. When $h = 2d$, the terminal velocity of TB increases over time due to the added mass effect and TB collides with LB before it enters the spiral motion. We also observe the central breakup of TB due to its elongation. When $h = 4d$, the two bubbles interact in the straight rising path and the transition phase. The same velocity oscillations are observed when TB is unaffected by LB. After that, the velocity of TB increases due to the interaction with LB, and the velocity oscillation of TB is bigger than that of LB. When $h = 6d$, the distance of the two bubbles is far enough that both yield path instability. The wake generated by LB can cause the lateral motion of TB (moving either toward the wake center or away from it), which depends on the position of TB in the wake of LB and the intensity of the vortices TB encounters. Compared to the case of single bubble, the liquid volume-averaged velocity created by two inline bubbles is doubled before TB enters the wake region of LB ($t' = 10$) and is less than the doubled value after TB enters the wake region of LB. The total liquid kinetic energy transferred from two inline bubbles is four times that from a single bubble before $t' = 10$ and less than the four times after that due to the wake effect of the LB.

ACKNOWLEDGMENTS

DATA AVAILABILITY

The data that support the findings of this study are available from the corresponding author upon reasonable request.

REFERENCES

[1]S. L. Anna, "Droplets and bubbles in microfluidic devices," Annu. Rev. Fluid Mech. **48**, 285–309 (2016).

[2]R. Zenit and J. R. Rodriguez, "The fluid mechanics of bubbly drinks," Phys. Today **71**(11), 44–50 (2018).

[3]M. K. Tripathi, K. C. Sahu, and R. Govindarajan, "Dynamics of an initially spherical bubble rising in quiescent liquid," Nat. Commun. **6**, 6268 (2015).

[4]Y. Cao and R. Macián-Juan, "Numerical study of the central breakup behaviors of a large bubble rising in quiescent liquid," Chem. Eng. Sci. **225**, 115804 (2020).

[5]O. Antepara, N. Balcázar, J. Rigola, and A. Oliva, "Numerical study of rising bubbles with path instability using conservative level-set and adaptive mesh refinement," Comput. Fluids **187**, 83–97 (2019).

[6]J. C. Cano-Lozano, C. Martinez-Bazan, J. Magnaudet, and J. Tchoufag, "Paths and wakes of deformable nearly spheroidal rising bubbles close to the transition to path instability," Phys. Rev. Fluids **1**, 053604 (2016).

[7]Y. Cao, I. M. Canals, and R. Macian-Juan, "Path instability of a compressible air bubble rising in quiescent water with consideration of variable thermophysical properties," Int. J. Multiphase Flow **129**, 103320 (2020).

[8]S. Winnikow and B. Chao, "Droplet motion in purified systems," Phys. Fluids **9**, 50–61 (1966).

[9]G. Ryskin and L. Leal, "Numerical solution of free-boundary problems in fluid mechanics. Part 2. Buoyancy-driven motion of a gas bubble through a quiescent liquid," J. Fluid Mech. **148**, 19–35 (1984).

[10]P. Duineveld, "The rise velocity and shape of bubbles in pure water at high Reynolds number," J. Fluid Mech. **292**, 325–332 (1995).

[11]A. Tomiyama, G. Celata, S. Hosokawa, and S. Yoshida, "Terminal velocity of single bubbles in surface tension force dominant regime," Int. J. Multiphase Flow **28**, 1497–1519 (2002).

[12]A. de Vries, A. Biesheuvel, and L. Van Wijngaarden, "Notes on the path and wake of a gas bubble rising in pure water," Int. J. Multiphase Flow **28**, 1823–1835 (2002).

[13]C. Veldhuis, A. Biesheuvel, and L. Van Wijngaarden, "Shape oscillations on bubbles rising in clean and in tap water," Phys. Fluids **20**, 040705 (2008).

[14]M. Wegener, J. Grünig, J. Stüber, A. Paschedag, and M. Kraume, "Transient rise velocity and mass transfer of a single drop with interfacial instabilities–experimental investigations," Chem. Eng. Sci. **62**, 2967–2978 (2007).

[15]M. Wegener, M. Kraume, and A. R. Paschedag, "Terminal and transient drop rise velocity of single toluene droplets in water," AIChE J. **56**, 2–10 (2009).

[16]M. Wegener, N. Paul, and M. Kraume, "Fluid dynamics and mass transfer at single droplets in liquid/liquid systems," Int. J. Heat Mass Transfer **71**, 475–495 (2014).

[17]H. Yuan and A. Prosperetti, "On the in-line motion of two spherical bubbles in a viscous fluid," J. Fluid Mech. **278**, 325–349 (1994).

[18]M. Watanabe and T. Sanada, "In-line motion of a pair of bubbles in a viscous liquid," JSME Int. J. Ser. B **49**, 410–418 (2006).

[19]J. Katz and C. Meneveau, "Wake-induced relative motion of bubbles rising in line," Int. J. Multiphase Flow **22**, 239–258 (1996).

[20]Y. Tagawa, S. Takagi, and Y. Matsumoto, "Surfactant effect on path instability of a rising bubble," J. Fluid Mech. **738**, 124 (2014).

[21]A. Senapati, G. Singh, and R. Lakkaraju, "Numerical simulations of an inline rising unequal-sized bubble pair in a liquid column," Chem. Eng. Sci. **208**, 115159 (2019).

[22]A. Kumar, B. Ray, and G. Biswas, "Dynamics of two coaxially rising gas bubbles," Phys. Fluids **33**, 052106 (2021).

[23]Y. Hallez and D. Legendre, "Interaction between two spherical bubbles rising in a viscous liquid," J. Fluid Mech. **673**, 406–431 (2011).

[24]M. Gumulya, R. Utikar, G. Evans, J. Joshi, and V. Pareek, "Interaction of bubbles rising inline in quiescent liquid," Chem. Eng. Sci. **166**, 1–10 (2017).

[25]H. Kusuno, H. Yamamoto, and T. Sanada, "Lift force acting on a pair of clean bubbles rising in-line," Phys. Fluids **31**, 072105 (2019).

[26]A. Filella, P. Ern, and V. Roig, "Interaction of two oscillating bubbles rising in a thin-gap cell: Ertical entrainment and interaction with vortices," J. Fluid Mech. **888**, A13 (2020).

[27]H. G. Weller, G. Tabor, H. Jasak, and C. Fureby, "A tensorial approach to computational continuum mechanics using object-oriented techniques," Comput. Phys. **12**, 620–631 (1998).

[28]S. S. Deshpande, L. Anumolu, and M. F. Trujillo, "Evaluating the performance of the two-phase flow solver interFoam," Comput. Sci. Discovery **5**, 014016 (2012).

[29]R. I. Issa, "Solution of the implicitly discretised fluid flow equations by operator-splitting," J. Comput. Phys. **62**, 40–65 (1986).

[30]J. Roenby, H. Bredmose, and H. Jasak, "A computational method for sharp interface advection," R. Soc. Open Sci. **3**, 160405 (2016).

[31]D. Sharaf, A. Premlata, M. K. Tripathi, B. Karri, and K. C. Sahu, "Shapes and paths of an air bubble rising in quiescent liquids," Phys. Fluids **29**, 122104 (2017).

[32]Y. Cao and R. Macián-Juan, "Numerical investigation of central breakup of large bubble induced by liquid jet," Phys. Fluids **32**, 033302 (2020).

[33]J. Zhang and M.-J. Ni, "What happens to the vortex structures when the rising bubble transits from zigzag to spiral?," J. Fluid Mech. **828**, 353–373 (2017).

[34]L. Liu, H. Yan, G. Zhao, and J. Zhuang, "Experimental studies on the terminal velocity of air bubbles in water and glycerol aqueous solution," Exp. Therm. Fluid Sci. **78**, 254–265 (2016).

[35]M. Gumulya, J. Joshi, R. Utikar, G. Evans, and V. Pareek, "Characteristics of energy production and dissipation around a bubble rising in water," Chem. Eng. Sci. **193**, 38–52 (2019).

[36]J. B. Joshi, K. Nandakumar, G. M. Evans, V. K. Pareek, M. M. Gumulya, M. J. Sathe, and M. A. Khanwale, "Bubble generated turbulence and direct numerical simulations," Chem. Eng. Sci. **157**, 26–75 (2017).

[37]M. Gumulya, R. Utikar, V. Pareek, G. Evans, and J. Joshi, "Dynamics of bubbles rising in pseudo-2d bubble column: Effect of confinement and inertia," Chem. Eng. J. **405**, 126615 (2021).

[38]J. Jeong and F. Hussain, "On the identification of a vortex," J. Fluid Mech. **285**, 69–94 (1995).

[39]J. Zhou, R. J. Adrian, S. Balachandar, and T. Kendall, "Mechanisms for generating coherent packets of hairpin vortices in channel flow," J. Fluid Mech. **387**, 353–396 (1999).

[40]Y. Zhang, K. Chen, Y. You, and W. Ren, "Coalescence of two initially spherical bubbles: Dual effect of liquid viscosity," Int. J. Heat Fluid Flow **72**, 61–72 (2018).

[41]H. Kusuno and T. Sanada, "Wake-induced lateral migration of approaching bubbles," Int. J. Multiphase Flow **139**, 103639 (2021).

[42]C. Brücker, "Structure and dynamics of the wake of bubbles and its relevance for bubble interaction," Phys. Fluids **11**, 1781–1796 (1999).